Hindawi
Complexity
Volume 2022, Article ID 3086747, 11 pages
https://doi.org/10.1155/2022/3086747

Research Article

A Hidden Chaotic Attractor with an Independent Amplitude-Frequency Controller

Yousuf Islam,[1,2] Chunbiao Li,[1,2] Yicheng Jiang,[1,2] Xu Ma,[1,2] and Akif Akgul[3]

[1]*School of Electronic Information Engineering, Nanjing University of Information Science & Technology, Nanjing 210044, China*
[2]*Jiangsu Collaborative Innovation Center of Atmospheric Environment and Equipment Technology (CICAEET), Nanjing University of Information Science & Technology, Nanjing 210044, China*
[3]*Department of Computer Engineering, Faculty of Engineering, Hitit University, Corum 19030, Turkey*

Correspondence should be addressed to Akif Akgul; akifakgul@hitit.edu.tr

Received 10 January 2022; Accepted 11 February 2022; Published 6 March 2022

Academic Editor: M. De Aguiar

In this paper, a three-dimensional chaotic system with a line equilibrium is studied, in which a single nonbifurcation parameter is used to control the amplitude and frequency. A variety of chaotic signals can be modified using the amplitude-frequency control switch. The realization of circuit simulation based on multisim further verifies the theoretical analysis. Finally, the method for encrypting color images is tested, and the process performance is valued. It shows that the novel chaotic oscillation has a promising application prospect in image encryption.

1. Introduction

Since chaos was first modeled by Edward Norton Lorenz in 1963 [1], great attention has been attracted for the reason that in such deterministic systems, chaos refers to the presence of seemingly random irregular motion [2]. In fact, chaos is a universal phenomenon in nonlinear systems and an inherent property of nonlinear dynamic systems. Chaos is a fundamental concept in nonlinear systems, and it is frequently used to characterize phenomena including bifurcation and periodic motion [3, 4]. It is found that a chaotic system will display bifurcation under specific parameters and that periodic and aperiodic motion can become entangled. Many famous 3-D chaotic systems have been proposed, including Arneodo systems, Sprott systems, Chen systems, Lv-Chen systems, Cai systems, and T systems [5–8]. A chaotic circuit is a significant research topic and an important representation of chaos. Chua proposed the first chaotic circuit in 1984 [9–12], trying to bridge the gap between chaos theory and chaotic circuits. People have performed significant research on chaos theory and produced numerous novel breakthroughs in recent years as a result of the wide application of chaos [13–17]. For information encryption, chaotic sequence signals have a significant application value. Chaos has been extensively applied for many aspects due to the intricate relationship between chaos and cryptography, and significant advancement has been performed in this area. Because of the irregularities and unpredictability of chaotic signals, chaos and corresponding fundamental systems have received a lot of attention [18–24]. A high-dimensional system's chaotic dynamics seem to be more complex, and sometimes, they show hyperchaos for more than two positive Lyapunov exponents [25, 26]. Therefore, it has been proven that chaotic signals can contribute to enhancing the security of chaos-based communication as well as digital encryption. Furthermore, a hidden chaotic attractor is an important phenomenon found ten years ago. The hidden oscillation has received a lot of attention because of its potential threat and possible applications. Finding hidden chaotic attractors in nonlinear dynamical systems has become a major issue in nonlinear dynamical system research [27–29]. Many hidden attractors have been found in memristive systems [30] and hyperchaotic systems [31]. However, there is not much attention on hidden attractors with amplitude-frequency control. Recently, Wang et al. [32]

studied the amplitude control and encryption application of chaotic signal, and they found that modular circuit cells with systematically configured parameters are useful for implementing multipiecewise Chua's diode. Wang et al. [33, 34] also studied the hidden oscillations in Chua's circuit and modified Sprott-A systems, where all the basins of attraction are not intersected with any equilibrium point indicating hidden attractor.

In this paper, a chaotic system with a line of equilibrium points is focused on, where the attractor stands in the region with negative y, and thus, the basin of attraction does not intersect with all equilibrium points indicating hidden attractor. Furthermore, the amplitude and frequency of hidden oscillation can be controlled by a single knob. Circuit implementation shows the convenience of amplitude-frequency control of the chaotic signal. Image encryption proves the merits of this system. The remaining of this paper is organized as follows. In Section 2, the system model is elaborated. In Section 3, the dynamics of the system are analyzed. In Section 4, the system is implemented in a simulated circuit. Finally, a chaotic system is applied to image encryption. The conclusions are presented in the last section.

2. A Novel Hidden Attractor

In reference [35], the 3-dimensional chaotic system is articulated as

$$\begin{cases} \dot{x} = cy + y^2 - ayz, \\ \dot{y} = -z^2 + byz, \\ \dot{z} = xy. \end{cases} \tag{1}$$

The system state variables are x, y, and z, while the constants a, b, and c are the real coefficients, with dots representing a derivative of time t. When $a = 0.9$, $b = 1$, $c = 1$, and IC = (2, −2, 2), the system (1) exhibits chaos in the region with negative y, as shown in Figure 1. There are six terms in this new system, with two nonlinear items. The Lyapunov exponents are $L_1 = 0.1314$, $L_2 = 0$, and $L_3 = -0.8453$.

3. Dynamical Analysis

3.1. Equilibrium Points. Let $\dot{x} = \dot{y} = \dot{z} = 0$. The equilibrium points of the system can be calculated as

$$\begin{cases} cy + y^2 - ayz = 0, \\ -z^2 + byz = 0, \\ xy = 0, \end{cases} \tag{2}$$

$$\begin{cases} E_O = x, 0, 0, \\ E_1 = 0, -c, 0, \\ E_2 = 0, \dfrac{c}{ab-1}, \dfrac{bc}{ab-1}, \end{cases} \tag{3}$$

where $a = 0.9$, $b = 1$, and $c = 1$. Solving this equation, the dynamical system (1) has three nontrivial equilibrium points in (2) which is independent of the value of the parameters a, b, and c.

$$J = \begin{vmatrix} 0 & c + 2y - az & -ay \\ 0 & bz & by - 2z \\ y & x & 0 \end{vmatrix}. \tag{4}$$

As $|J - \lambda I| = 0$, the characteristic equation is

$$\det(J - \lambda I) = -a\lambda y^2 + 2ayz^2 + bcy^2 + b\lambda^2 z + b\lambda xy + 2by^3 - 2cyz - \lambda^3 - 2\lambda xz - 4y^2 z = 0. \tag{5}$$

In the Jacobian matrix of system (1), the equilibrium point E is defined as

$$J(E_O) = J(E_1) = J(E_2) = \begin{pmatrix} 0 & c + 2y - az & -ay \\ 0 & bz & by - 2z \\ y & x & 0 \end{pmatrix}. \tag{6}$$

The eigenvalues of the matrix at the equilibrium point can be determined as follows:

$$\begin{cases} E_O\colon \lambda_1 = 0; \lambda_2 = 0; \lambda_3 = 0, \\ E_1\colon \lambda_1 = -0.7113; \lambda_2 = 0.3556 + 1.1311i; \lambda_3 = 0.3556 - 1.1311i, \\ E_2\colon \lambda_1 = 0.9911; \lambda_2 = -5.4956 + 8.4079i, \lambda_3 = -5.4956 - 8.4079i. \end{cases} \tag{7}$$

The eigenvalues of the system are obtained while $a = 0.9$, $b = 1$, and $c = 1$. The obtained all eigenvalues are given in Equation (7). The equilibrium $E_1(0, -c, 0)$ is a saddle-focus point of index-2; therefore, this equilibrium point E_1 is unstable, and we can see in E_2 that λ_1 is a positive real number, and λ_2 and λ_3 are a pair of complex conjugate

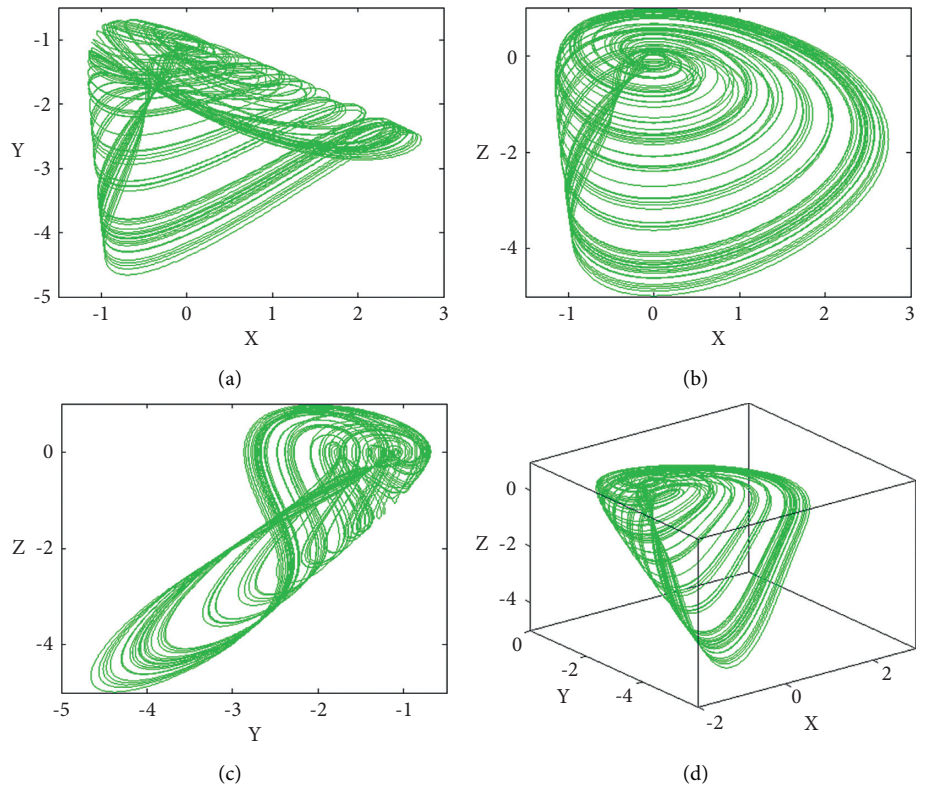

FIGURE 1: Chaotic attractor of system (1) with $a = 0.9$, $b = 1$, and $c = 1$ under initial condition IC = (2, − 2, 2): (a) (x)-(y), (b) (x)-(z), (c) (y)-(z), and (d) (x)-(y)-(z).

eigenvalues with a negative real number. The equilibrium $E_2(0, c/ab - 1, bc/ab - 1)$ is a saddle-focus point of index-1; therefore, this equilibrium point E_2 is also unstable.

3.2. Dissipativity Analysis. Inference μ is a region in the horizontal surface A^3, and $V(t)$ is set to be the volume of $\mu(t)$.

Here, we obtain

$$\dot{V}(t) = \int_{\mu(t)}^{\infty} (\nabla \times F) \mathrm{d}x\mathrm{d}y\mathrm{d}z. \tag{8}$$

Therefore, the dissipativity of the proposed chaotic system is

$$\begin{aligned} \nabla \times F &= \frac{\partial \dot{x}}{x} + \frac{\partial \dot{y}}{y} + \frac{\partial \dot{z}}{z}, \\ &= \frac{\partial\left(cy + y^2 - ayz\right)}{x} + \frac{\partial\left(-z^2 + byz\right)}{y} + \frac{\partial(xy)}{z} \\ &= 0 + bz + 0 = z = \gamma, \end{aligned} \tag{9}$$

where F is the 3-dimensional chaotic system, and b and z are the real parameters. The above equation is rewritten as

$$\dot{V}(t) = \int_{\mu(t)}^{\infty} \gamma \mathrm{d}x\mathrm{d}y\mathrm{d}z = \gamma V(t). \tag{10}$$

Therefore, we can obtain $V(t) = e^{\gamma} V(0)$; if $\nabla \times F < 0$, then system (1) is dissipative and the state of the system is bounded by the state of the system (when a = 0.9, b = 1, and c = 1).

3.3. Amplitude and Frequent Control. In system (1), parameter c is a single knob for amplitude and frequency control. Let $x \longrightarrow mx$, $y \longrightarrow my$, $z \longrightarrow mz$, $t \longrightarrow t/m$ $(m > 0)$; then, system (1) turns to be

$$\begin{cases} \dot{x} = \dfrac{c}{m} y + y^2 - ayz, \\ \dot{y} = -z^2 + byz, \\ \dot{z} = xy, \end{cases} \tag{11}$$

indicating that the parameter c can control the amplitude and frequency of all variables x, y, and z, as shown in Figure 2. In Figure 3(a), when the linear coefficient c is increased, system (1) keeps the chaotic state of all the time and the chaotic area continue to increase. The rescaled amplitude and frequency can also be proved by Lyapunov exponents, as shown in Figure 3(b).

4. Circuit Implementation

Circuit verification is also an essential step in the implementation of the proposed chaotic system to ensure its

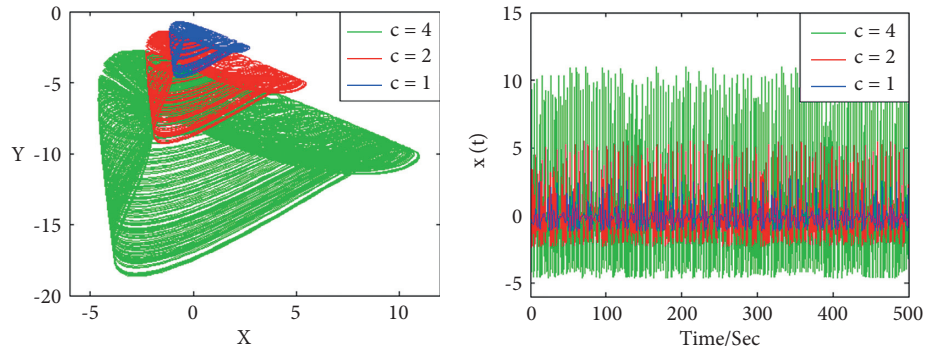

Figure 2: Rescaled attractor of system (1) with $a = 0.9$, $b = 1$, and initial values (2, −2, 2) under the parameter c: (a) (x)-(y) and (b) signal $x(t)$.

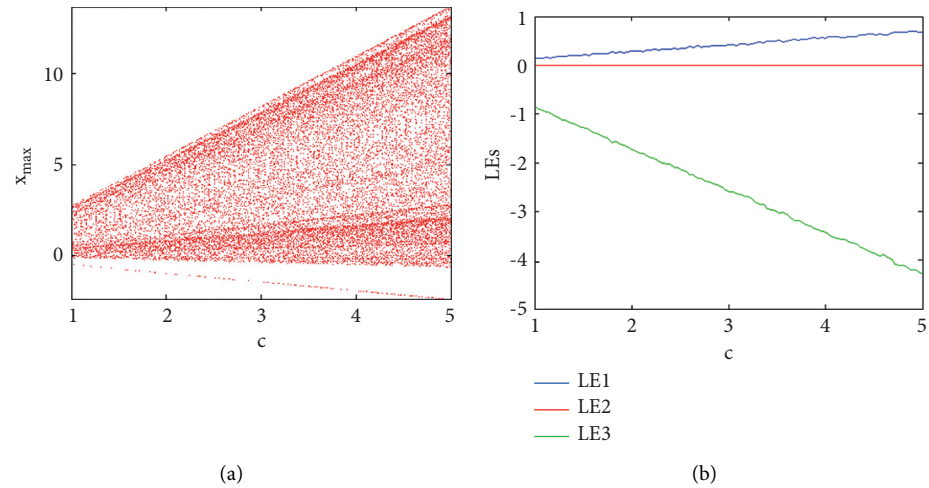

Figure 3: Dynamical evolution of system (1) with $a = 0.9$, $b = 1$, and initial values (2, − 2, 2) when c is in [1, 5]: (a) bifurcation diagram and (b) Lyapunov exponents.

correctness. Meanwhile, the key issue in the circuit is how to implement a circuit expression for a 3D chaotic system by converting and transforming it into a realistic circuit using electronic devices such as capacitors and resistors. To authenticate the efficiency of our proposed 3-dimensional chaotic system, the circuit implementation is designed and simulated with the NI multisim circuit simulation software, and the simulation results are detailed in this section.

For this circuit construction, it is transformed to be

$$\begin{cases} \dot{x} = \dfrac{1}{R_1 C_1} y + \dfrac{1}{R_2 C_1} y^2 - \dfrac{1}{R_3 C_1} yz, \\ \dot{y} = -\dfrac{1}{R_4 C_2} z^2 + \dfrac{1}{R_5 C_2} yz, \\ \dot{z} = \dfrac{1}{R_8 C_3} xy. \end{cases} \tag{12}$$

A chaotic system is defined as a system that has several causes and multiplication, addition, and differentiation, and differentiation exists in the system equations, and a realistic expression of this system is obtained utilizing a summation, an integrator, and a transformer. The relevant circuit implementation is depicted in Figure 4 based on the above explanations. The state variables x, y, and z in the system (1) correspond to the state voltages of the capacitors C_1, C_1, and C_3 in the simplified circuit, and the corresponding circuit components can be selected as follows: $V_1 = V_2 = 15V$, $C_1 = C_2 = C_3 = 10nF$, $R_1 = R_2 = R_4 = R_5 = R_6 = R_7 = R_8 = 100k\Omega$, $R_3 = 106k\Omega$; LM741CN is selected as an operational amplifier; there is a general time scale 1000 for better displaying in the oscilloscope.

Figure 5 shows the phase trajectory of the system (1) in the analog oscilloscope. The area of the phase track will change with the organization of the resistance R_1, as shown in Figure 5(d).

5. Application in Image Encryption

The chaotic system with a linear equilibrium in this section has a higher level of unpredictability, a larger keyspace, and a higher level of complexity, all of which make the encryption stronger secure in concept.

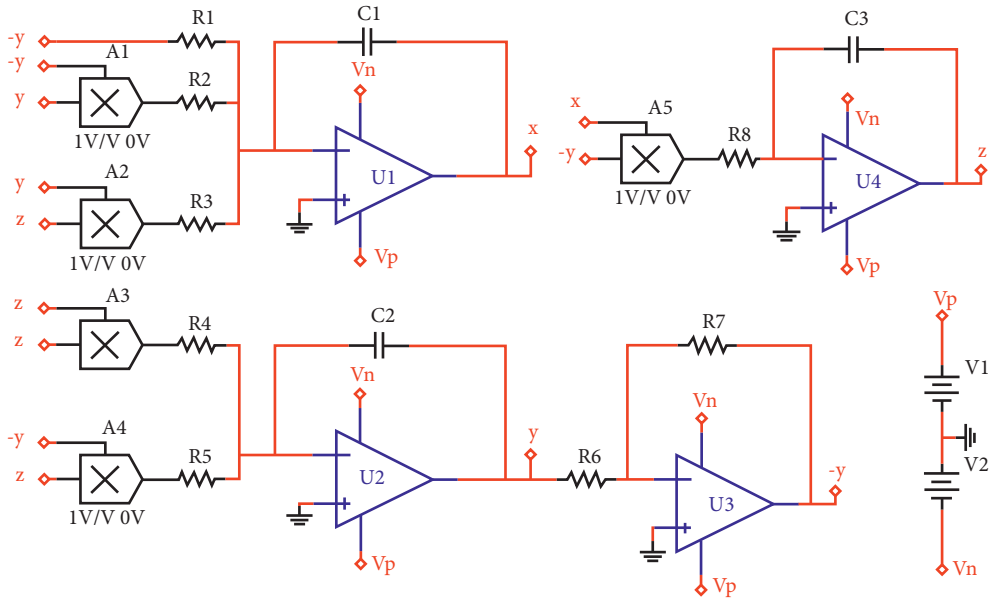

Figure 4: Circuit realization of the system (1).

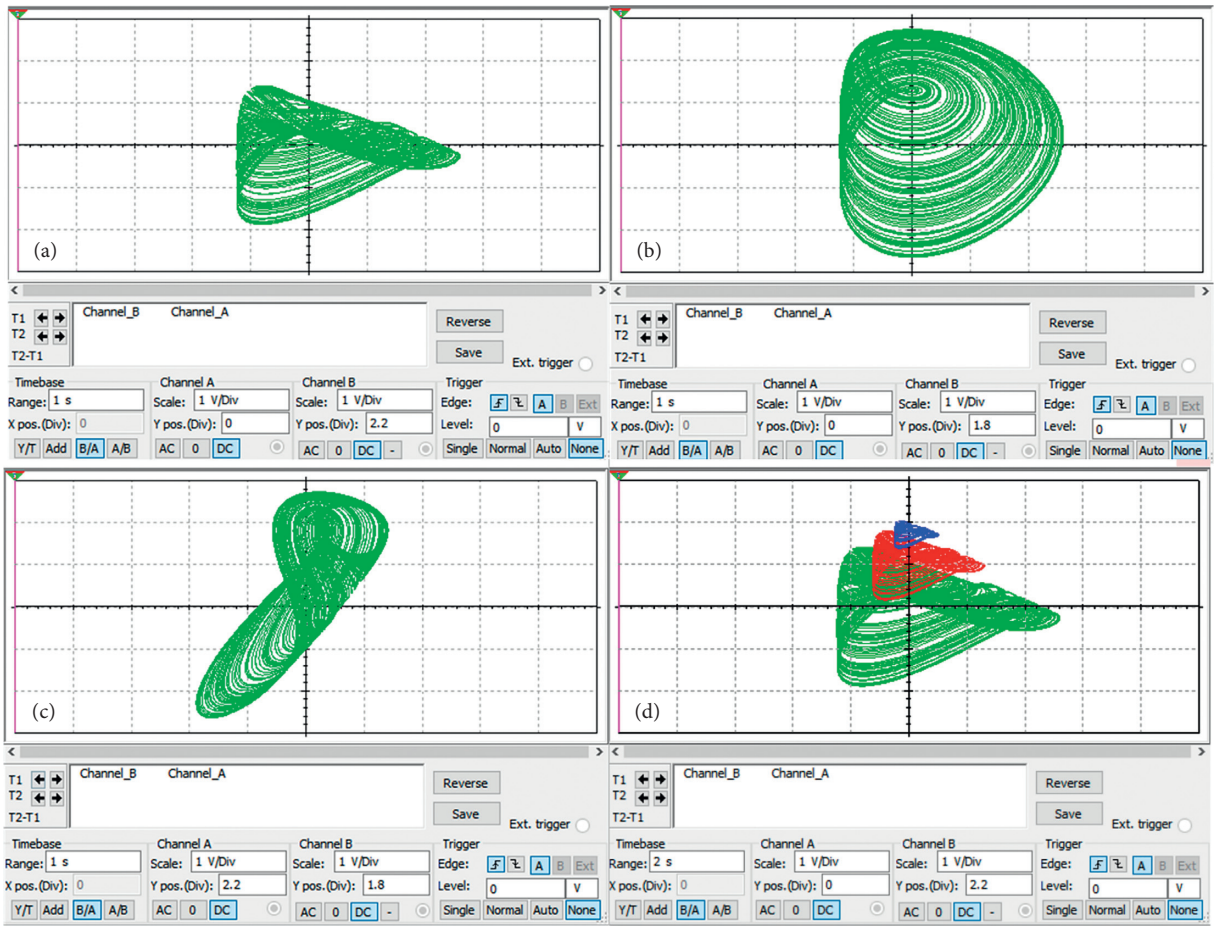

Figure 5: Chaotic attractor of system (1): (a) (x)-(y), (b) (x)-(z), (c) (y)-(z), and (d) the attractor changes due to the difference of R_1 resistance.

5.1. Encryption Application with a Chaotic System. The control parameters and initial conditions of the system are (Table 1) $\mu = 3.9999$ and $x_0 = 0.6209$, respectively, and a standard color image is chosen for testing, as illustrated in Figure 6. The new chaotic system parameters are $a = 0.9$, $b = 1$, and $c = 1$. The initial conditions are set as $X_0 = 0.7361, Y_0 = 0.4663, Z_0 = 0.1501$, and $U_0 = 0.7653$. Table 2 describes the selected keys that were chosen. M_1 and N_1 are the zeroing parameters used throughout encryption; k_1 is the average gray level of G in the original image, and the original image k_2 is the average gray level of B. Figure 6(b) shows the encrypted image after simulation. The image after encryption is chaotic and fundamentally different from the image before processing, as it can be observed. The properly decrypted image, which can be seen in Figure 6(c), is identical to the original image (Table 2).

5.2. Security Analysis. Secure analysis is the most essential and fundamental requirement for an encrypted system. In general, a chaotic image encryption algorithm requires a substantial keyspace, reversible encryption and decryption, strong antiattack characteristics, and the other performances, and then the performance of chaos-based encryption is the next to determine by using the following eligibility requirements: keyspace analysis, histogram analysis, information entropy analysis, and correlation analysis.

5.3. Keyspace Analysis. The keyspace can approach $(10^{16})^{10} = 10^{160}$, satisfying the security level of the keyspace (greater than 2^{128}) using a 64-bit processor, floating-point precision up to 10^{-16}. The modified system can be observed to be more resistant to the attacker's comprehensive attack. The decrypted image cannot be acquired accurately when the algorithm key is changed slightly, as shown in Figure 7. As a result, the new system has a high level of key sensitivity. The images used throughout the investigations are 256×256 conventional images with a $2^3 = 8$-bit grayscale.

5.4. Histogram Analysis. The distribution of pixel intensity values within an image is represented by a histogram. It can be utilized to defend against statistical attacks. The frequency distribution of each gray level pixel can be visually displayed using a gray histogram, which is a statistical analytical method. The histogram of the image becomes smooth even after encryption, compared to the fluctuation before encryption, thus preventing the attacker from accessing the original image information through statistical analysis, resulting in information leakage, and ensuring information. Figures 8(a)–8(c) are the histograms of the original image, and Figures 8(d)–8(f) are the histograms of the encrypted images. It is clear that the new system can withstand a more powerful onslaught.

5.5. Information Analysis for Entropy. The image's information entropy can be used to evaluate the level of uncertainty and randomness in the image distribution of its pixel gray value. Typically, the higher the image's entropy, the more consistent the image's gray distribution. In a grayscale image, each pixel is coded in 8 bits. As a result, an image's maximum entropy value is 8. The information entropy of the encrypted image should be near 8, which indicates the best amount of uncertainty, owing to a decent encryption process. To compute the information entropy, many users use the method as follows:

$$\text{entropy}H(m) = -\sum_{i=1}^{H} p(x_i)\log_2\ p(x_i), \tag{13}$$

where $p(x_i)$ represents the probability of the occurrence of the gray value x_i and H indicates the gray level of the image. Theoretically, for a completely random digital image with a grayscale of 256 has an evenly distributed pixel value in [0, 255], then $p(x_i) = 1/256$ $(i \in \in [0, 255])$, and the estimated information entropy is 8 bits. If the image is encrypted, the closer the image's information entropy is near 8, the better the encryption features.

5.6. Correlation Statistical Analysis. On the one hand, the correlation level of adjacent pixels is larger when the correlation coefficient degree of adjacent pixels is higher. On the other hand, the lower the correlation, the smaller the coefficient. As a result, calculating the correlation coefficient can be justified the algorithm's security. The lower the correlation and the advanced security, the smaller the coefficient. The correlation coefficients were calculated from the three channels (R, G, and B) with three directions: horizontal, vertical, and diagonal, to measure the correlation between the original image and adjacent pixels of the ciphertext image; N pairs of adjacent pixels were selected from the image, and the correlation coefficients were calculated from the three channels (R, G, B) with three directions: horizontal, vertical, and diagonal. To equivalence the autocorrelation of an unadorned and encrypted image, we have calculated the correlation coefficient r of each pair of pixels by using the following formula:

$$\begin{aligned} r_{XY} &= \frac{\text{cov}(X,Y)}{\sqrt{D(X)D(Y)}}, \\ E(X) &= \frac{1}{N}\sum_{i=1}^{N}(x_i), \\ D(X) &= \frac{1}{N}\sum_{i=1}^{N}(x_i - E(X)), \\ \text{cov}(X,Y) &= \frac{1}{N}\sum_{i=1}^{N}(x_i - E(X))(y_i - E(Y)), \end{aligned} \tag{14}$$

where $\text{cov}(X,Y)$ represents the correlation and autocorrelation function, X and Y are the grayscale values of two adjacent pixels in the image, and N denotes the sample. E is the expected value operator, and $D(X)$ represents the variance of the variable x. The values of r_{XY} lie in the range

Table 1: Algorithm key.

Key	μ	x_0	X_0	Y_0	Z_0	U_0	M_1	N_1	k_1	k_2
Value	3.9999	0.6209	0.7361	0.4663	0.1501	0.7653	0	0	0.4761	0.1255.

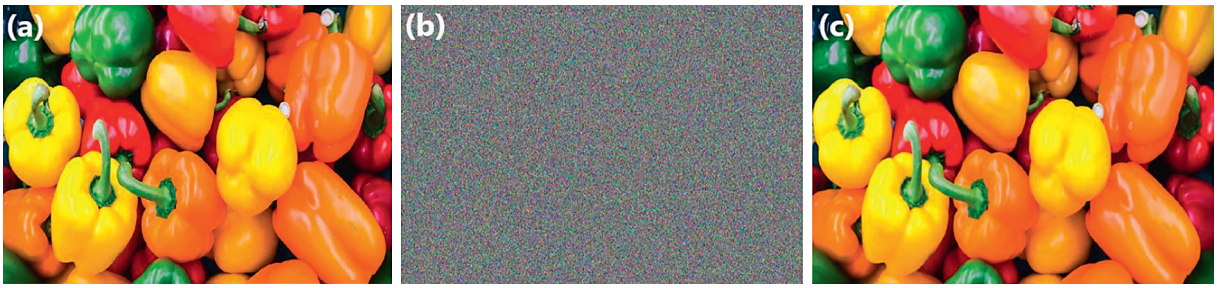

Figure 6: Encryption images: (a) original pepper image; (b) encryption pepper image; (c) decryption pepper image.

Table 2: The information entropy of the three channels in the original and encrypted on the pepper image.

Image	R channel entropy	G channel entropy	B channel entropy
Original picture	5.6871	7.6856	4.686
Encrypted image	7.9997	7.9997	7.9998

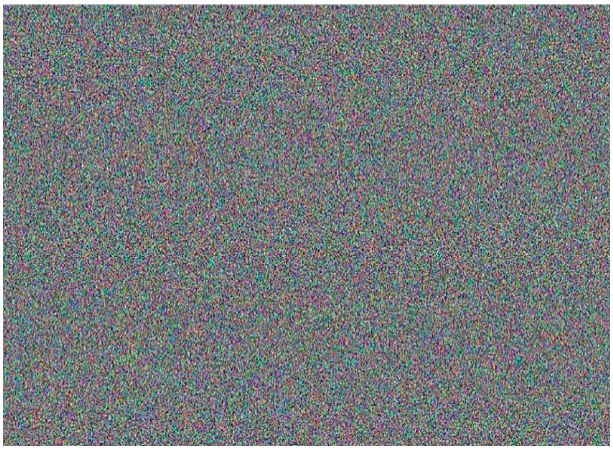

Figure 7: Initial condition perturbation ciphertext.

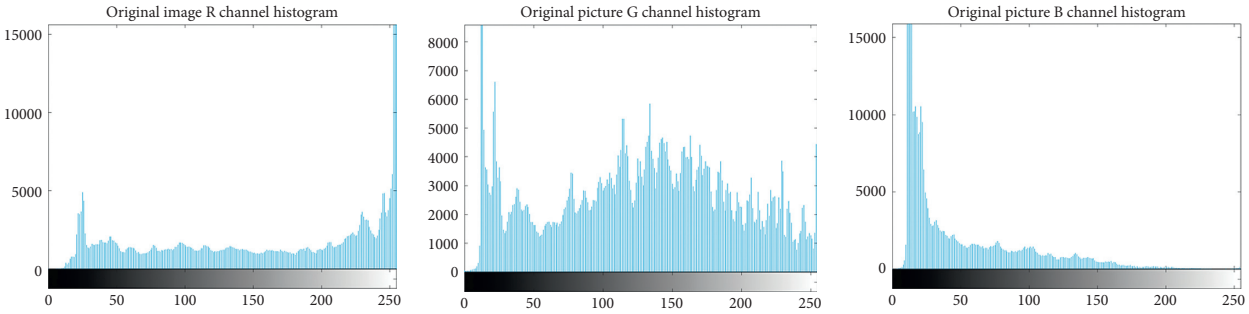

(a) (b) (c)

Figure 8: Continued.

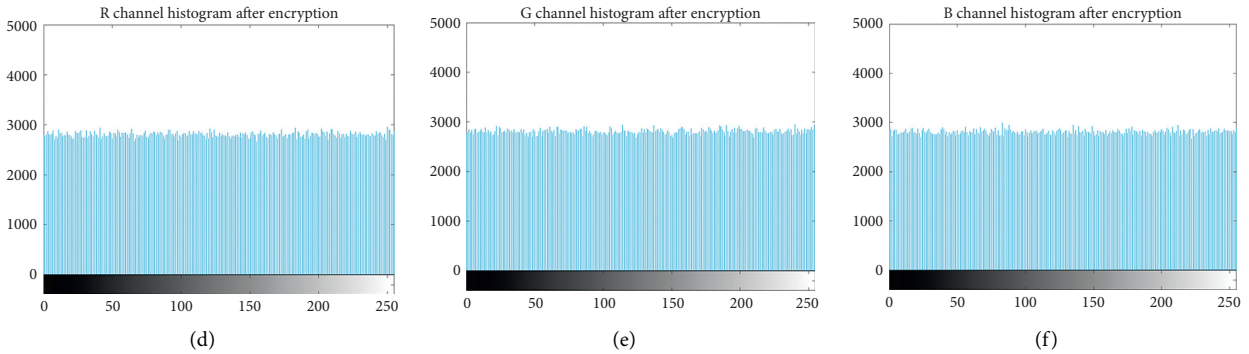

Figure 8: Histogram experiment images. (a–c) Histogram of the original image. (d–f) Histogram of the encrypted image.

Table 3: A correlation coefficient of two adjacent pixels in the original and encrypted on the pepper image.

Image	Channel	Horizontal	Vertical	Diagonal
Original image	B	0.98645	0.98782	0.97851
	G	0.99529	0.99282	0.98965
	R	0.99428	0.99168	0.98792
Encrypted image	B	0.00494	−0.02531	0.00540
	G	−0.01262	−0.01606	0.00444
	R	−0.00282	−0.01656	0.00919

Table 4: Correlation coefficient test result [36].

Image	Channel	Horizontal	Vertical	Diagonal
Original image	Red	0.97489	0.98660	0.96227
	Green	0.97532	0.98731	0.96377
	Blue	0.95167	0.97112	0.92931
Encrypted image	Red	0.00070	0.01175	0.01539
	Green	0.00855	−0.01537	−0.01660
	Blue	0.00122	0.00135	0.01235

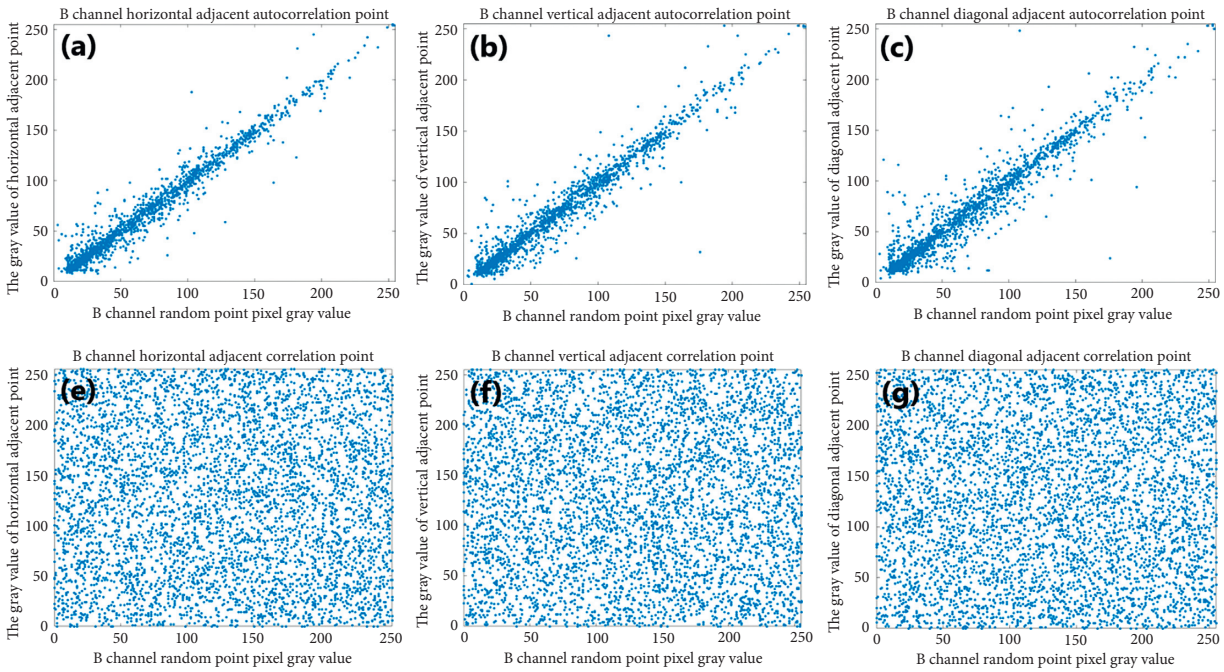

Figure 9: Correlation and autocorrelation of R channel adjacent pixels of the pepper image and its ciphered image: (a) horizontal direction of the pepper image; (b) vertical direction of the pepper image; (c) diagonal direction of the pepper image; (d) horizontal direction of the pepper ciphered image; (e) vertical direction of the pepper ciphered image; (f) diagonal direction of the pepper ciphered image.

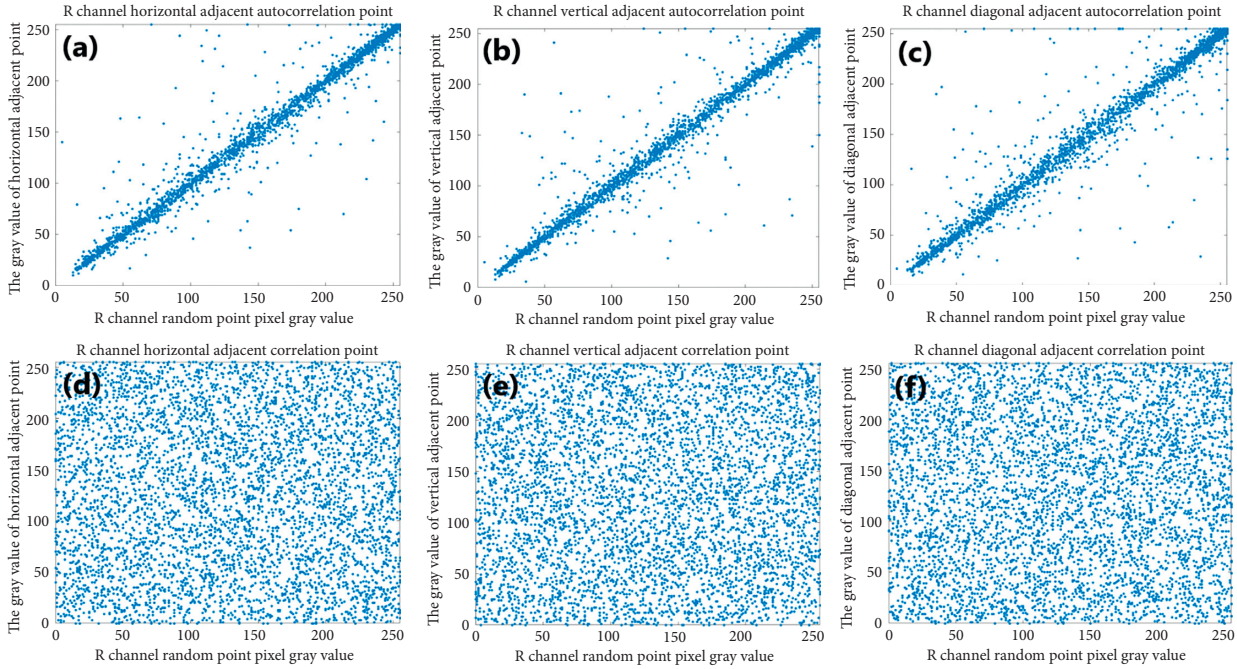

Figure 10: Correlation and autocorrelation of G channel adjacent pixels of the pepper image and its ciphered image: (a) horizontal direction of the pepper image; (b) vertical direction of the pepper image; (c) diagonal direction of the pepper image; (d) horizontal direction of the pepper ciphered image; (e) vertical direction of the pepper ciphered image; (f) diagonal direction of the pepper ciphered image.

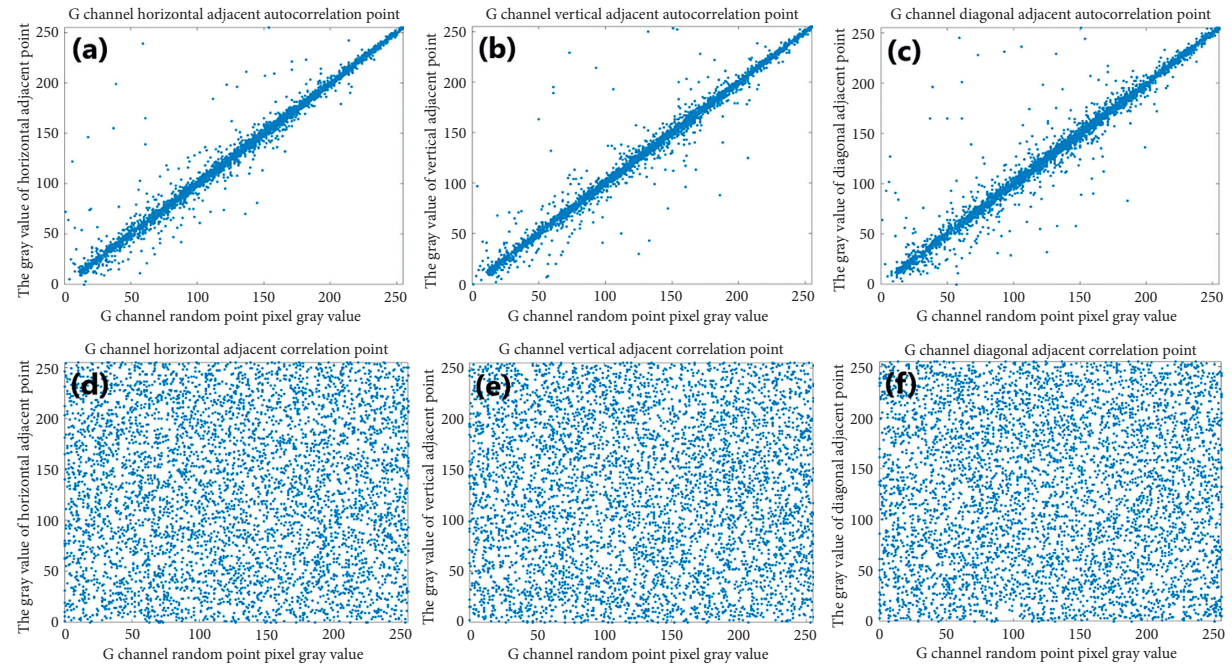

Figure 11: Correlation and autocorrelation of B channel adjacent pixels of the pepper image and its ciphered image: (a) horizontal direction of the pepper image; (b) vertical direction of the pepper image; (c) diagonal direction of the pepper image; (d) horizontal direction of the pepper ciphered image; (e) vertical direction of the pepper ciphered image; (f) diagonal direction of the pepper ciphered image.

[−1, 1], with 1 indicating perfect correlation, −1 indicating anticorrelation, and 0 representing no correlation.

Here, we can see from Table 3 that the correlation coefficients of the original image are all very close to 1, whereas the correlation coefficients of the encrypted image are all very close to 0, indicating that the encrypted image's pixel point distribution is very highly discrete.

If we compare Tables 3 and 4 with each other, we can see some different points. In Table 3, the original correlation coefficient values are average horizontal 99.2%, vertical

99.07%, and diagonal 98.54%, and in Table 4, the original correlation coefficient values are average horizontal 96.72%, vertical 98.17%, and diagonal 95.18%, that is, the original points in Table 3 are closer to 1 and the encrypted points are also closer to 0 than Table 4. So, Table 3 indicates that the encrypted points of distribution are highly discrete.

The correlation and autocorrelation plots for each image are shown in Figures 9–11. In Table 3, horizontal, vertical, and diagonal directions provide their correlation and autocorrelation coefficients. Table 3 also includes significant data from references for comparison.

6. Conclusion

The single nonbifurcation parameter of the system can effectively modify the amplitude and frequency of the demonstrated three-dimensional chaotic system. Numerical simulation and circuit experiment based on multisim agree to each other by proving the phenomenon. As a typical application, the property of image encryption is exhaustively analyzed. With the chaotic signal from the new system, a color image is well encrypted and decrypted in the keyspace. Histogram and correlation of adjacent pixels are used for showing the high encryption performance.

Data Availability

The data used to support the findings of this study are available from the corresponding author upon reasonable request.

Conflicts of Interest

The authors declare that there are no conflicts of interest regarding the publication of this paper.

References

[1] E. N. Lorenz, "Deterministic nonperiodic flow," *J. Atoms*, vol. 20, pp. 25–36, 1963.

[2] W. Yu, J. Wang, J. Wang et al., "Design of a new seven-dimensional hyperchaotic circuit and its application in secure communication," *IEEE Access*, vol. 7, pp. 125586–125608, 2019.

[3] C. Li, J. C. Sprott, W. Hu, and Y. Xu, "Infinite multistability in a self-reproducing chaotic system," *International Journal of Bifurcation and Chaos*, vol. 27, no. 10, Article ID 1750160, 2017.

[4] C. Li, W. Li, J. Zhang, Y. Xie, and Y. Zhao, "Amplitude-phase modulation, topological horseshoe and scaling attractor of a dynamical system," *Communications in Theoretical Physics*, vol. 66, no. 9, pp. 297–305, 2016.

[5] G. Chen and T. Ueta, "Yet another chaotic attractor," *International Journal of Bifurcation and Chaos*, vol. 9, no. 7, pp. 1465-1466, 1999.

[6] J. Lü and G. Chen, "A new chaotic attractor coined," *International Journal of Bifurcation and Chaos*, vol. 12, no. 3, pp. 659–661, 2002.

[7] J. Lü, G. Chen, D. Cheng, and S. Celikovsky, "Bridge the gap between the lorenz system and the chen system," *International Journal of Bifurcation and Chaos*, vol. 12, no. 12, pp. 2917–2926, 2002.

[8] Q. Yang, G. Chen, and T. Zhou, "A unified Lorenz-Type system and its canonical form," *International Journal of Bifurcation and Chaos*, vol. 16, no. 10, pp. 2855–2871, 2006.

[9] L. O. Chua, T. Matsumoto, and M. Komuro, "The double scroll family. 2. rigorous analysis of bifurcation phenomena," *IEEE Transactions on Circuits and Systems*, vol. 33, no. 11, pp. 1097–1118, 1986.

[10] Z. Wei, P. Yu, W. Zhang, and M. Yao, "Study of hidden attractors, multiple limit cycles from Hopf bifurcation and boundedness of motion in the generalized hyperchaotic Rabinovich system," *Nonlinear Dynamics*, vol. 82, no. 1-2, pp. 131–141, 2015.

[11] A. Akgul, S. Hussain, and I. Pehlivan, "A new three-dimensional chaotic system, its dynamical analysis and electronic circuit applications," *Optik*, vol. 127, no. 18, pp. 7062–7071, 2016.

[12] Z. Wei, V.-T. Pham, T. Kapitaniak, and Z. Wang, "Bifurcation analysis and circuit realization for multiple-delayed Wang-Chen system with hidden chaotic attractors," *Nonlinear Dynamics*, vol. 85, no. 3, pp. 1635–1650, 2016.

[13] S. M. Tabatabaie Nezhad, M. Nazari, and E. A. Gharavol, "A novel dos and ddos attacks detection algorithm using arima time series model and chaotic system in computer networks," *IEEE Communications Letters*, vol. 20, no. 4, pp. 700–703, 2016.

[14] Z. Wei, I. Moroz, J. C. Sprott, Z. Wang, and W. Zhang, "Detecting hidden chaotic regions and complex dynamics in the self-exciting homopolar disc dynamo," *International Journal of Bifurcation and Chaos*, vol. 27, no. 2, Article ID 1730008, 2017.

[15] J. P. Singh and B. K. Roy, "The simplest 4-D chaotic system with line of equilibria, chaotic 2-torus and 3-torus behaviour," *Nonlinear Dynamics*, vol. 89, no. 3, pp. 1845–1862, 2017.

[16] Z. Wang, A. Akgul, V. T. Pham, and S. Jafari, "Chaos-based application of a novel no-equilibrium chaotic system with coexisting attractors," *Nonlinear Dynamics*, vol. 89, no. 46, pp. 1877–1887, 2017.

[17] J. P. Singh and B. K. Roy, "Second order adaptive time varying sliding mode control for synchronization of hidden chaotic orbits in a new uncertain 4-D conservative chaotic system," *Transactions of the Institute of Measurement and Control*, vol. 40, no. 13, pp. 3573–3586, 2018.

[18] J. P. Singh, K. Lochan, N. V. Kuznetsov, and B. K. Roy, "Coexistence of single- and multi-scroll chaotic orbits in a single-link flexible joint robot manipulator with stable spiral and index-4 spiral repellor types of equilibria," *Nonlinear Dynamics*, vol. 90, no. 2, pp. 1277–1299, 2017.

[19] Z. Wei, I. Moroz, J. C. Sprott, A. Akgul, and W. Zhang, "Hidden hyperchaos and electronic circuit application in a 5d self-exciting homopolar disc dynamo," *Chaos: An Interdisciplinary Journal of Nonlinear Science*, vol. 27, no. 3, Article ID 033101, 2017.

[20] V. R. F. Signing and J. Kengne, "Coexistence of hidden attractors, 2-torus and 3-torus in a new simple 4-D chaotic system with hyperbolic cosine nonlinearity," *International Journal of Dynamics and Control*, vol. 6, pp. 421–1428, 2018.

[21] S. Vaidyanathan, A. Sambas, S. Kacar, and Ü. Çavuşoğlu, "A new three-dimensional chaotic system with a cloud-shaped curve of equilibrium points, its circuit implementation and sound encryption," *International Journal of Modelling, Identification and Control*, vol. 30, no. 3, pp. 184–196, 2018.

[22] Z. Wei, V. T. Pham, A. J. M. Khalaf, J. Kengne, and S. Jafari, "A modified multistable chaotic oscillator," *International Journal*

of Bifurcation and Chaos in Applied Sciences and Engineering, vol. 28, no. 7, Article ID 1850085, 2018.

[23] A. Akgül, S. Kaçar, B. Arıcıoğlu, and I. Pehlivan, "Text encryption by using one-dimensional chaos generators and nonlinear equations," in *Proceedings of the 2013 8th International Conference on Electrical and Electronics Engineering (ELECO)*, pp. 320–323, IEEE, Bursa, Turkey, November 2013.

[24] K. Rajagopal, V. T. Pham, F. R. Tahir, A. Akgul, H. R. Abdolmohammadi, and S. Jafari, "A chaotic jerk system with non-hyperbolic equilibrium: dynamics, effect of time delay and circuit realisation," *Pramana*, vol. 90, no. 4, pp. 1–8, 2018.

[25] X. Zhang, C. Li, Y. Chen, H. H. C. Iu, and T. Lei, "A memristive chaotic oscillator with controllable amplitude and frequency," *Chaos, Solitons & Fractals*, vol. 139, Article ID 110000, 2020.

[26] C. Li, J. C. Sprott, A. Akgul, H. H. C. Iu, and Y. Zhao, "A new chaotic oscillator with free control," *Chaos: An Interdisciplinary Journal of Nonlinear Science*, vol. 27, no. 8, Article ID 083101, 2017.

[27] G. A. Leonov, N. V. Kuznetsov, and V. I. Vagaitsev, "Localization of hidden Chua's attractors," *Physics Letters A*, vol. 375, no. 23, pp. 2230–2233, 2011.

[28] G. A. Leonov, N. V. Kuznetsov, and V. I. Vagaitsev, "Hidden attractor in smooth Chua systems," *Physica D: Nonlinear Phenomena*, vol. 241, no. 18, pp. 1482–1486, 2012.

[29] S. Vaidyanathan, A. T. Azar, A. Akgul, C. H. Lien, S. Kacar, and U. Cavusoglu, "A memristor-based system with hidden hyperchaotic attractors, its circuit design, synchronisation via integral sliding mode control and an application to voice encryption," *International Journal of Automation and Control*, vol. 13, no. 6, pp. 644–667, 2019.

[30] S. Zhang, J. Zheng, X. Wang, and Z. Zeng, "Multi-scroll hidden attractor in memristive HR neuron model under electromagnetic radiation and its applications," *Chaos: An Interdisciplinary Journal of Nonlinear Science*, vol. 31, no. 1, Article ID 011101, 2021.

[31] Q. Yang, L. Yang, and B. Ou, "Hidden hyperchaotic attractors in a new 5D system based on chaotic system with two stable node-foci," *International Journal of Bifurcation and Chaos*, vol. 29, no. 7, Article ID 1950092, 2019.

[32] N. Wang, C. Li, H. Bao, M. Chen, and B. Bao, "Generating multi-scroll chua's attractors via simplified piecewise-linear chua's diode," *IEEE Transactions on Circuits and Systems I: Regular Papers*, vol. 66, no. 12, pp. 4767–4779, 2019.

[33] N. Wang, G. Zhang, N. V. Kuznetsov, and H. Bao, "Hidden attractors and multistability in a modified Chua's circuit," *Communications in Nonlinear Science and Numerical Simulation*, vol. 92, Article ID 105494, 2021.

[34] N. Wang, G. Zhang, N. V. Kuznetsov, and H. Li, "Generating grid chaotic sea from system without equilibrium point," *Communications in Nonlinear Science and Numerical Simulation*, vol. 107, Article ID 106194, 2022.

[35] C. Li and J. C. Sprott, "Chaotic flows with a single nonquadratic term," *Physics Letters A*, vol. 378, no. 3, pp. 178–183, 2014.

[36] J. Sun, C. Li, T. Lu, A. Akgul, and F. Min, "A memristive chaotic system with hypermultistability and its application in image encryption," *IEEE Access*, vol. 8, pp. 139289–139298, 2020.